Journal of
Manufacturing and Materials Processing

MDPI

Article

Dissimilar MIG Welding Optimization of C20 and SUS201 by Taguchi Method

Thanh Tan Nguyen [1], Van Huong Hoang [1], Van-Thuc Nguyen [1,*] and Van Thanh Tien Nguyen [2,*]

[1] Faculty of Mechanical Engineering, Ho Chi Minh City University of Technology and Education, Ho Chi Minh City 71307, Vietnam
[2] Faculty of Mechanical Engineering, Industrial University of Ho Chi Minh City, Nguyen Van Bao Street, Ward 4, Go Vap District, Ho Chi Minh City 70000, Vietnam
* Correspondence: nvthuc@hcmute.edu.vn (V.-T.N.); thanhtienck@gmail.com or nguyenvanthanhtien@iuh.edu.vn (V.T.T.N.)

Abstract: This study looks at how welding intensity, speed, voltage, and stick-out affect the structural and mechanical characteristics of metal inert gas (MIG) welding on SUS 201 stainless steel and C20 steel. The Taguchi method is used to optimize the study's experiment findings. The results show that the welding current has a more significant effect on the tensile test than the welding voltage, stick-out, and welding speed. Welding voltage has the lowest influence. In addition to the base metals' ferrite, pearlite, and austenite phases, the weld bead area contains martensite and bainite microstructures. The optimal parameters for the ultimate tensile strength (UTS), yield strength, and elongation values are a 110 amp welding current, 15 V of voltage, a 500 mm.min^{-1} welding speed, and a 10 mm stick-out. The confirmed UTS, yield strength, and elongation values are 452.78 MPa, 374.65 MPa, and 38.55%, respectively, comparable with the expected value derived using the Taguchi method. In the flexural test, the welding current is the most critical element affecting flexural strength. A welding current of 110 amp, an arc voltage of 15 V, a welding speed of 500 mm.min^{-1}, and a stick-out of 12 mm are the ideal values for flexural strength. The flexural strength, confirmed at 1756.78 MPa, is more than that of the other samples. The study's conclusions can offer more details regarding the dissimilar welding industry.

Keywords: taguchi method; ANOVA; C20; SUS201; tensile test; bending test; microstructure

Citation: Nguyen, T.T.; Hoang, V.H.; Nguyen, V.-T.; Nguyen, V.T.T. Dissimilar MIG Welding Optimization of C20 and SUS201 by Taguchi Method. *J. Manuf. Mater. Process.* **2024**, *8*, 219. https://doi.org/10.3390/jmmp8050219

Received: 18 August 2024
Revised: 19 September 2024
Accepted: 25 September 2024
Published: 1 October 2024

1. Introduction

Carbon steel C20, also known as low-carbon steel, is widely used in the mechanical and construction industries. Its notable characteristics include high ductility, good tensile strength, and reasonable costs [1]. Stainless steel SUS201 is austenitic stainless steel belonging to the chromium–nickel–manganese family, widely utilized across various industries due to its excellent properties and cost-effectiveness. The outstanding feature of SUS201 is its good corrosion resistance, particularly in humid environments or when exposed to mild chemicals [2]. Welding wire GM70S AWS A5. 18 ER70S-6 Standard is widely used in the MIG welding process due to its outstanding characteristics and versatile applications. GM70S also has high tensile strength and good crack resistance. It is suitable for welding carbon steel and low-alloy steel materials in heavy industrial applications, such as steel structure fabrication, automotive manufacturing, shipbuilding, and machinery production [3]. Dissimilar welding between low-carbon steel C20 and SUS201 steel with GM70S, therefore, could provide high-quality welding joints.

To create metallic bodies with multi-purposes, such as lightweight, high corrosion resistance, high-strength, and low-cost, welding two different metals or alloys is commonly considered [4–7]. This technique is called dissimilar welding, a vital manufacturing method in automobiles, chemical and petrochemical industries, power generation, and electronics.

Dissimilar welding can be applied to connect copper–steel, steel–aluminum, aluminum–copper, and steel–nickel, using some specific welding technology such as MIG, Tungsten Inert Gas (TIG), laser welding (LW), friction stir welding (FSW), plasma arc welding, and electron beam welding [8–10]. Creating dissimilar welding between stainless and low-carbon steels plays an important role in manufacturing structures such as automobiles, chemical and petrochemical industries, and power generation [11]. Moreover, carbon steel pipes are commonly used in domestic and industrial settings to weld with stainless steel tanks to transport water or other liquid solutions [12]. Coal-fired boilers and other power industries, such as dissimilar welding structures for connecting the pipe nozzle of a reactor pressure vessel to the safe-end pipe, are commonly employed in carbon steel and stainless steel dissimilar welding [13,14]. Compared to other methods, MIG welding is usually applied due to the low cost of equipment and good welding quality [15]. MIG welding has several disadvantages. For example, the MIG welding process is sensitive to the wind as the gas shield can be impacted by wind, reducing the welding quality [16]. The accessibility is also limited due to the size and rigidity of the welding gun [17].

Besides some merits, the welding joints of dissimilar welding have some critical demerits, such as thermal expansion mismatch, corrosion, weldability, high brittleness, and process control [18–21]. The welding of stainless steel and low-carbon steel has been the subject of significant research due to its wide range of applications. Studies have investigated the joining of AISI 304, 316, 309, and 201 stainless steels with SS400, AISI 1020, 1018 low-carbon steel, and galvanized steel using various welding processes like TIG, shielded metal arc welding (SMAW), LW, FSW, and MIG. The research has focused on understanding the influence of welding parameters, post-weld heat treatment, and heat input on the resulting joint properties, including UTS, microstructures, and microhardness [22–26]. For example, the joining between AISI 304 stainless steel and low carbon steel (LCS) was investigated at varying welding speeds. The microstructure and corrosion performance of weldment by gas metal arc welding (GMAW) with an ER309 L wire electrode were studied [22]. GMAW examined the UTS of the dissimilar welded connections between 304 stainless steel (SUS304) and SS400 LCS. Four welding parameters, including the welding current, arc voltage, and welding speed, were examined [23]. The AISI 304 stainless steel and low carbon steel were welded using a process to examine the effects of the current, speed, and gas flow rate on the mechanical properties and microstructure of the weldments [24]. The welding junction between mild steel (MS) of grade AISI 1020 and stainless steel (SS) of grade AISI 304 was completed using the TIG and SMAW techniques. MS and SS filler materials were used to examine the impact of filler material in the dissimilar welding joint. Three different temperatures, 600 °C, 630 °C, and 650 °C, were examined for post-weld heat treatment over the welded specimens [25]. The mechanical characteristics and weld-bead shape of the gas metal arc dissimilar weld joints of LCS and AISI 304 stainless steel were optimized in Abioye et al.'s report [26]. They surveyed the wire feed rate, welding voltage, and welding speed. They all significantly impact the tensile strength and hardness of the weld joint. The optimal parameters are a wire feed rate of 84 mm/s, a welding voltage of 25 V, and a welding speed of 3 mm/s, generating a high UTS value of 422 MPa and a hardness of 112 HB.

Khdir et al. examined the effects of various heat inputs on the microstructure and mechanical characteristics of dissimilar welding between low-carbon steel and austenitic stainless steel (AISI 304), joined by using a CO_2 4 kW laser welding. Five distinct heat inputs—0.5, 0.9, 1.41, 2, and 2.5 KJ.mm^{-1}—were used to examine the mechanical characteristics and microstructure of the welded zone [27]. In addition, laser welding was used to join the dissimilar austenitic stainless steel (AISI 316) and LCS (AISI 1018) without the need for a filler metal. Next, research was performed on how post-weld heat treatment affected the distribution of Ni and Cr in welded joints and their microstructure, tensile and yield strength, microhardness, and phase composition in the weld zone [28]. The effects of laser welding process parameters on different weld joints were examined with different laser powers, welding speeds, and a constant shielding gas flow rate. After investigation, the

differences in the mechanical characteristics and microstructures of the heat-affected and dissimilar weld zones were discovered [29]. Moreover, the process of double-sided butt joint friction stir welding was used to fuse specimens of carbon steel and stainless steel 316. The study examined the impact of tool rotation speed and specimen preheat temperature on the mechanical behavior and microstructure that emerged [30]. Furthermore, Arc stud welding was used to attach AISI 1020 carbon steel sheets to AISI 309 stainless steel studs. Various welding currents and periods were used to determine how welding parameters affected the microstructure and mechanical characteristics of the weldments [31]. Furthermore, MIG welding was used to unite stainless steel 201 with galvanized steel. The goal of this study was to find out what the maximum load may be on a different joint. Three levels are employed for each parameter: gas pressure, welding wire speed, and welding speed [32].

The Taguchi method is a statistical technique created by Dr. Genichi Taguchi to raise the Standard of produced products. It is commonly known as a robust design approach and is widely applied in industry and by scholars [33–35]. For example, Benlamnouar et al. [36] used the Taguchi method to optimize the dissimilar welding parameters between X70-304 L steel. The results demonstrated that, in dissimilar joints, hardness has a stronger correlation with microstructural evolution than tensile strength. It was found that the most critical TIG welding parameter influencing the different weld qualities is gas flow. Notably, Ramarao et al. [37] studied the impact strength of GMAW dissimilar welding between SA387 steel and SS304 steel. They also applied the Taguchi method to optimize the welding parameters. The results showed that welding current was the most critical parameter in determining the impact strength, followed by the bevel angle and welding voltage. Behera et al. [38] investigated the optimization process of dissimilar welding between 316 L stainless steel and medium carbon steel generated by the laser method. The welding parameters, including scanning speed, spot size, and pulse frequency, are surveyed. The optimal parameters are a scanning speed of 45 mm/min, a spot size of 0.3 mm, and a pulse frequency of 7 Hz, leading to the weld hardness of 304.8 HV and heat-affected zone length of 85.2 μm. Ogedengbe et al. [24] welded low-carbon steel and AISI 304 stainless steel using a gas tungsten arc dissimilar process within a process window to study the effects of gas flow rate (GFR), speed, and current on the mechanical properties and microstructure of the pieces. The result showed that the UTS (ranging between 428 and 886 MPa) varied directly with the GFR but inversely with the current and welding speed. The optimum UTS was obtained at the current of 110 A, welding speed of 37.5 mm/min, and GFR of 15 L/min. In all samples, the weld region exhibited higher hardness (297–396 HV) than the heat-affected zone (HAZ) in the base metals (maximum of 223 $\pm$ 6 HV).

Despite these investigations, identifying a desirable welding quality through optimization necessitates additional research. Firstly, welding voltage, current, speed, and stick-out distance are rarely optimized simultaneously despite their substantial impact on the welding quality. Secondly, the flexural strength of the weld joint is often ignored. Therefore, this study investigated the effects of welding voltage, current, speed, and stick-out distance on the tensile strength and flexural strength of the dissimilar welding between low-carbon steel C20 and SUS 201 using the GMAW technique. Analysis is also performed on the dissimilar weld joint' microstructure. The Taguchi method designs the experiment's conditions to optimize the results. The study's findings may provide valuable insights into the dissimilar welding field, particularly in parameter selection and optimization.

2. Materials and Methods

2.1. Materials and Welding Parameters

Figure 1 shows the study's procedure to analyze and optimize the parameters affecting the weld quality, such as tensile strength, yield strength, elongation, and bending strength.

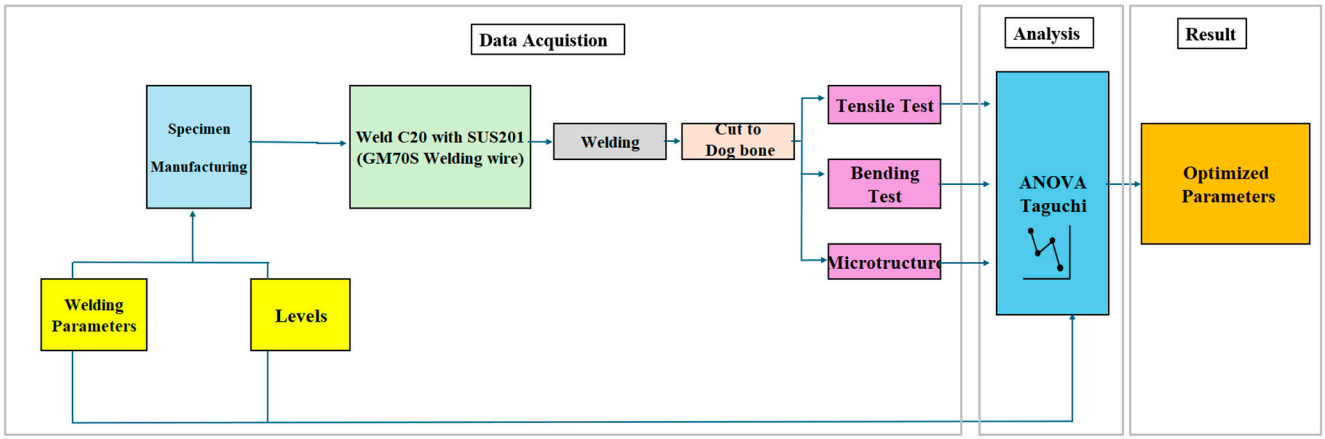

Figure 1. Flowchart of the experimental work.

The nominal chemical compositions and mechanical properties of SUS201 steel, C20 steel, and GM70S filler are shown in Tables 1–3. Material composition certificate, certified to meet quality standards of previous projects as outlined in [1,2]. GM70S filler was chosen for this study because it is available and more affordable than other filler types [39]. The steel sheets are prepared with the size of 110 mm × 105 mm × 2 mm. They are fixed using a jig fixture before welding, as presented in Figure 2. Tensile test samples were made in compliance with ASTM E290 standards, while bending test samples were produced following ASTM E8/E8M-13 standards (Figure 3). The dissimilar welding joints are conducted using a six-arm axes Robot Panasonic named TA-1400G2 series YA-1NA (Panasonic, Osaka, Japan). The travel angle is selected as 0°, the working angle is 90°, and the gas flow rate is 12 L/min. The shielding gases used in the process were Argon. Then, tensile test and bending are prepared for microstructure, bending, and tensile tests (Figure 4).

Table 1. Chemical composition and mechanical properties of C20 steel grade.

Grade	C	Si	Mn	P	S	Cu	Cr
C20	0.185%	0.007%	0.525%	0.0138%	0.009%	0.01%	0.026
	Tensile Strength (MPa)		Yield Strength (MPa)			Elongation (%)	
	402		245			28	

Table 2. Chemical composition and mechanical properties of SUS 201 Stainless Steel.

Grade	C	Si	Mn	P	S	Ni	Cr	N
SUS201	0.1225%	0.5588%	5.014%	0.0425%	0.0122%	4.43%	16.42.%	0.11%
	Tensile Strength (MPa)			Yield Strength (MPa)			Elongation (%)	
	515			260			40	

Table 3. Chemical composition and mechanical properties of AWS A5.18 ER70S-6 filler.

Grade	C	Mn	Si	P	S	Cr
AWS A5. 18 ER70S-6	0.07	1.48	0.83	0.011	0.015	0.11
	Tensile Strength (MPa)		Yield Strength (MPa)		Elongation (%)	
	550		450		30	

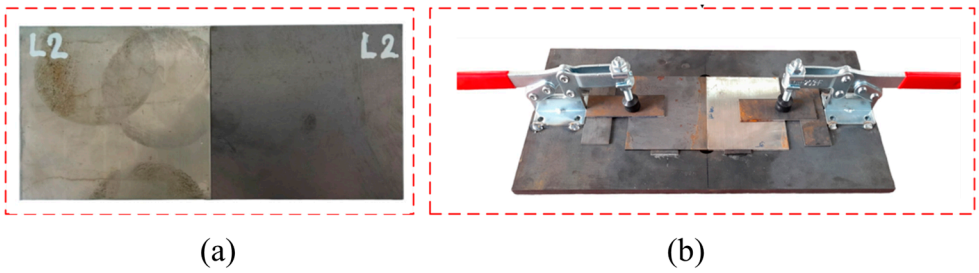

Figure 2. Workpieces fixed on the technological jig. (**a**) C20 and SUS201 samples, (**b**) fixture with clamp.

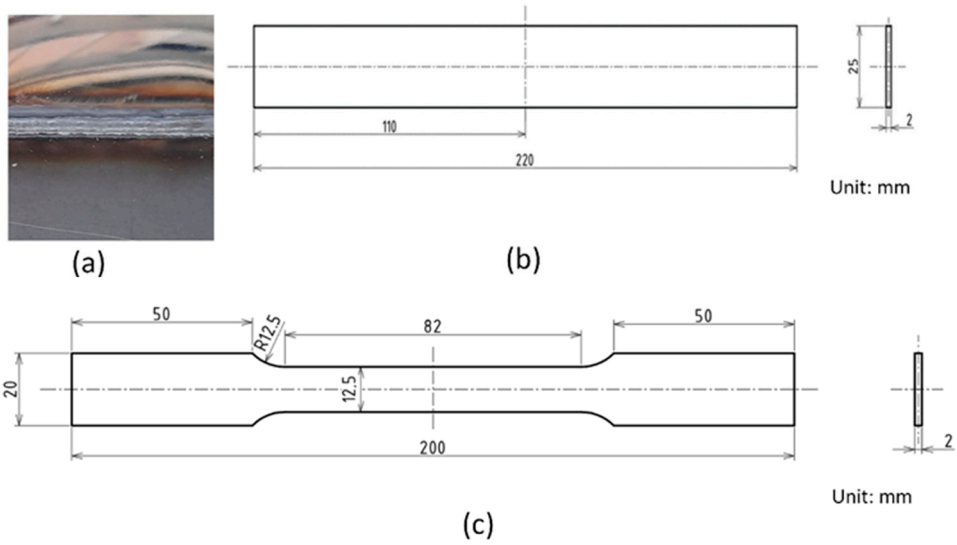

Figure 3. Dissimilar weld joints and testing shapes: (**a**) dissimilar welding sheet, (**b**) bending test shape according to ASTM E8/E8M-13 standard [40], and (**c**) tensile test shape according to ASTM E290 standard [41].

Firstly, the parameters are checked to ensure good welding quality and avoid serious flaws. Following that, the initial welding parameters are determined, as seen in Table 3. Four parameters, including welding voltage, welding current, welding speed, and electrical stick out, are used to design the welding parameters. The welding parameters created using the Taguchi approach are displayed in Table 4. The mechanical properties are the average of the three test samples for each number. The error was calculated using the mean deviation method [42].

Table 4. Welding process parameters and levels in dissimilar welding with GM70S filling wire.

Factors	Parameters	Level 1	Level 2	Level 3	Level 4
A	Welding Current—I (A)	80	90	100	110
B	Welding Voltage—U (V)	15	16	17	18
C	Electrical Stick-out—d (mm)	10	12	14	16
D	Welding Speed—v (mm.min^{-1})	450	500	550	600

Following welding, an electrical discharge wire-cutting machine is then used to precisely cut tensile test samples from the dissimilar weld sheet, which follows the ASTM E290 standard for tensile test samples and ASTM E8/E8M-13 standard for flexural sample shape [40,41]. Tensile samples are examined using the WE1000B universal testing machine (Jinan, Shandong, China). The chemical compositions of the base materials are tested via a PDA-700 spectrometer (Shimadzu, Kyoto, Japan). The samples' microstructure is studied using a metallurgical microscope Oxion OX.2153-PLM EUROMEX (Euromex Microscope

bv, Arnhem, The Netherlands). The microstructure of the dissimilar weld joints is prepared by cutting, machining, polishing, and etching with 4% HNO_3 or HCl/HNO_3 solution.

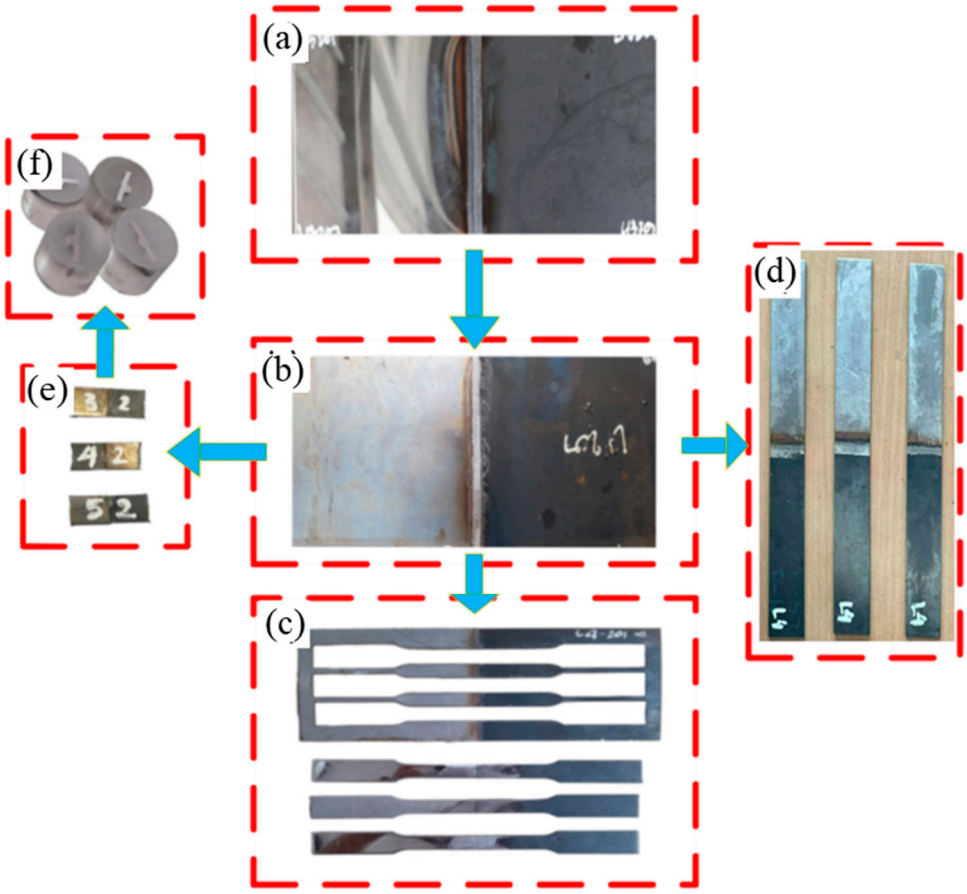

Figure 4. Prepare steps for tensile and bending test samples, including welding and preparing samples for microstructure, bending, and tensile tests. (**a**) weld dissimilar SUS201 and C20 steel, (**b**) weld is manufactured, (**c**) tensile test weld sample, (**d**) bending test sample preparation, (**e**) microstructure test preparation, and (**f**) microstructure test sample.

2.2. Parameters and Levels

The "Larger-the-better" criteria are selected to maximize the quality of dissimilar welding joints' quality. The S/N ratio is built and converted as [33]

$$S/N = -10\log\left(\frac{1}{n}\sum_{i=1}^{n}\frac{1}{y_i^2}\right) \quad (1)$$

The experiments were conducted in a planned order using the Taguchi L16 orthogonal array design. Four levels were considered for each input parameter, as shown in Table 4. As mentioned above, some initial experiments were conducted to select the range of parameters, ensuring that the maximum and minimum values were close to the limits at which the welds fail. The welding design matrix following the Taguchi L16 array is presented in Table 5.

Table 5. Experimental layout using the L16 orthogonal array and results.

No	Input Parameters					Output Parameters			
	I	U	d	v	Heat input	UTS	YS	L_f	FS
	(A)	(V)	(mm)	(mm.min^{-1})	(J.mm^{-1})	(MPa)	(MPa)	(%)	(MPa)
1	80	15	10	450	128.0	307.39 ± 14.5	246.74	10.39	912.99
2	80	16	12	500	122.9	181.46 ± 10.1	161.67	7.09	477.11
3	80	17	14	550	118.7	136.42 ± 10.8	123.43	6.46	296.82
4	80	18	16	600	115.2	216.34 ± 11.8	196.55	7.62	328.68
5	90	15	12	550	117.8	292.52 ± 13.6	236.21	10.37	833.62
6	90	16	10	600	115.2	256.92 ± 12.8	231.24	9.78	827.95
7	90	17	16	450	163.2	252.93 ± 11.6	217.53	9.4	399.33
8	90	18	14	500	155.5	276.04 ± 13.8	249.28	16.37	604.31
9	100	15	14	600	120.0	308.22 ± 16.4	216.53	21.13	1057.12
10	100	16	16	550	139.6	269.14 ± 12.5	212.76	12.35	731.0
11	100	17	10	500	163.2	386.37 ± 21.3	266.9	32.63	986.22
12	100	18	12	450	192.0	354.01 ± 16.7	262.58	28.46	1499.36
13	110	15	16	500	158.4	366.52 ± 14.5	262.87	36.36	1501.71
14	110	16	14	450	187.7	388.29 ± 19.3	279.2	42.25	1343.39
15	110	17	12	600	149.6	367.18 ± 15.4	263.22	38.25	1599.02
16	110	18	10	550	172.8	310.68 ± 16.5	257.04	36.06	1109.84

3. Results and Discussion

3.1. Tensile and Bending Test Results

Table 5 presents the tensile test results with UTS, yield strength, and elongation at break values. Interestingly, at sample number 14, the highest UTS of 388.29 MPa, the highest yield strength of 279.2 MPa, and the highest elongation of 42.25% were obtained at welding current 110 A, welding voltage 16 V, electrical stick-out 14 mm, and speed 450 mm.min^{-1}. Remarkably, three essential properties in the tensile test are obtained simultaneously at sample No. 14, indicating the advanced high quality of this sample to the other samples. In reverse, at sample number three, the lowest UTS, yield strength, and elongation were measured as 136.42 MPa, 123.43 MPa, and 6.46% at welding current 80 A, welding voltage 17 V, electrical stick-out 14 mm, and speed 550 mm.min^{-1}. This sample "No." shows the low quality of the dissimilar welding joints. As can be seen in Table 5, the highest flexural strength of 1599.02 MPa is sample No. 15, at welding current 110 A, welding voltage 17 V, electrical stick-out 12 mm, and speed 600 mm.min^{-1}. On the contrary, the lowest flexural strength is 296.82 MPa, compared to sample No. 3, which has the parameters of welding current 80 A, welding voltage 17 V, electrical stick-out 14 mm, and speed 550 mm.min^{-1}.

3.2. Taguchi Analysis

Unlike traditional methods involving numerous random experiments, the Taguchi method employs orthogonal arrays to strategically select a minimal set of experiments. This systematic approach ensures the most critical information is obtained while minimizing experimental effort. Consequently, the overall research duration and expenses are substantially decreased [43]. The objective is to maximize mechanical properties. Therefore, this study chose the S/N ratio related to the quality characteristic "Larger—the—Better." The results are calculated using Minitab 18 software, shown in Table 6.

Table 6 demonstrates that the welding current has the most significant effect on the tensile strength values, followed by the welding speed, stick-out, and welding voltage. Thus, adjusting the welding current could result in the appropriate UTS, yield strength, and elongation values for the dissimilar weld connection between SUS 201 and C20. This behavior is because increasing the welding current directly increases the heat input rate. The welding voltage, on the other hand, has the lowest impact rate due to the small examination rank of this study. Moreover, in the elongation results, the delta value of the welding current is 14.2, which is significantly higher than the other parameters, as

presented in Table 6, indicating its strong impact on the elongation value. Compared to the other parameters, the differences in the delta values are not high, suggesting that despite having different rankings, the dissimilarity is minor. These results indicate the relative balance of these parameters on the tensile test properties of the dissimilar welding joints between SUS 201 and C20.

Table 6. Response table for S/N and significance for tensile strength, yield strength, elongation, and flexural strength.

Tensile Strength (MPa)				
Response table for signal-to-noise ratios—Larger is better				
Level	Current (A)	Voltage (V)	Stick-out (mm)	Speed (mm.min^{-1})
1	46.08	50.03	49.88	50.14
2	48.6	48.44	49.19	49.25
3	50.27	48.45	48.27	47.62
4	51.05	49.09	48.66	48.99
Delta	4.97	1.6	1.61	2.53
Rank	1	4	3	2
Yield Strength (MPa)				
Response table for signal-to-noise ratios—Larger is better				
Level	Current (A)	Voltage (V)	Stick-out (mm)	Speed (mm.min^{-1})
1	44.92	47.6	47.96	47.97
2	47.36	46.73	47.11	47.26
3	47.54	46.38	46.35	46.01
4	48.48	47.59	46.88	47.06
Delta	3.56	1.23	1.62	1.96
Rank	1	4	3	2
Elongation (%)				
Response table for signal-to-noise ratios—Larger is better				
Level	Current (A)	Voltage (V)	Stick-out (mm)	Speed (mm.min^{-1})
1	17.43	24.59	26.39	26.35
2	20.97	22.79	24.52	26.69
3	26.92	24.03	24.51	22.01
4	31.63	26.54	22.54	23.9
Delta	14.2	2.74	2.85	3.69
Rank	1	4	3	2
Flexural Strength (MPa)				
Response table for signal-to-noise ratios—Larger is better				
Level	Current (A)	Voltage (V)	Stick-out (mm)	Speed (mm.min^{-1})
1	53.14	60.41	59.59	59.33
2	56.11	57.94	59.9	58.15
3	60.29	56.36	57.03	56.51
4	62.77	57.6	56.79	58.31
Delta	9.63	4.05	4.1	2.82
Rank	1	3	2	4

Table 6 shows that the welding current has the most significant effect on the flexural strength values, similar to the tensile test results. Following the highest impact of the welding current are stick-out, welding voltage, and welding speed. The ranking orders of these parameters are different from the tensile test results. After the welding, the welding speed, stick-out, and voltage effects are the current effects. Interestingly, the delta values of these parameters are close, indicating a slight difference in the mechanical impact. Controlling the welding current could generally lead to the desired flexural strength values for the dissimilar weld connection between SUS 201 and C20.

Applying the Taguchi optimization method, ANOVA tables for mean and signal-to-noise ratio are listed in Table 7. The F-test is conducted to assess the significance of process parameters. A high F-value indicates that the factor significantly affects the process response. In this study, welding current is the most critical factor and contributes the most to the weld's tensile strength, yield strength, elongation, and flexural strength. Moreover,

the p-value of the welding current is less than 0.05. This parameter statistically influences the tensile strength at the 95% confidence level. Remarkably, compared to other studies, welding current is the factor that has the most significant impact on the tensile strength yield strength, elongation, and flexural strength, contributing 63.47%, 50.37%, 83.41%, and 68.47%, respectively. On the contrary, welding voltage has the lowest impact level.

Table 7. ANOVA results for tensile strength, yield strength, elongation, and flexural strength.

ANOVA Results for Tensile Strength.						
Source	DF	Adj SS	Adj MS	F-Value	p-Value	Contribution (%)
Current (A)	1	50,627	50,627	29.93	0.00	63.47
Voltage (V)	1	1168	1168	0.69	0.424	1.46
Stick-out (mm)	1	3857	3857	2.28	0.159	4.84
Speed (mm.min^{-1})	1	5503	5503	3.25	0.099	6.9
Error	11	18,605	1691			23.33
Total	**15**	79,760				**100**
S = 41.1257		R-sq: 76.67%		R-sq(adj): 68.19%		
				$\sigma_{tensile} = \mathbf{207 + 5.046}I - \mathbf{7.84}U - \mathbf{6.97}d - \mathbf{0.333}v$		(2)
ANOVA results for yield strength.						
Current (A)	1	13,244.4	13,244.4	16.19	0.002	50.37
Voltage (V)	1	0.7	0.7	0	0.977	0.002
Stick-out (mm)	1	1949.5	1949.5	2.38	0.151	7.41
Speed (mm.min^{-1})	1	2098.9	2098.9	2.57	0.138	7.98
Error	11	9000.9	818.3			34.23
Total	**15**	26,294.5				100
S = 28.6053		R-sq: 66.77%		R-sq(adj): 53.32%		
				$\sigma_{yield} = \mathbf{161 + 2.573}I - \mathbf{0.19}U - \mathbf{4.94}d - \mathbf{0.205}v$		(3)
ANOVA results for elongation.						
Current (A)	1	2160.39	2160.39	83.18	0	83.41
Voltage (V)	1	26.37	26.37	0.98	0.344	0.98
Stick-out (mm)	1	58.4	58.4	2.25	0.162	2.25
Speed (mm.min^{-1})	1	60.15	60.15	2.32	0.156	2.32
Error	11	286.71	26.97			11.03
Total	**15**	2590.02				100
S = 6.09642		R-sq: 88.97%		R-sq(adj): 84.96%		
				$L_f = \mathbf{-67.8 + 1.039}I + \mathbf{1.13}U - \mathbf{0.854}d - \mathbf{0.0347}v$		(4)
ANOVA results for flexural strength.						
Current (A)	1	1,867,390	1,867,390	36.33	0	68.47
Voltage (V)	1	71,330	71,330	1.35	0.27	2.62
Stick-out (mm)	1	174,220	174,220	3.3	0.097	6.39
Speed (mm.min^{-1})	1	32,966	32,966	0.62	0.446	1.21
Error	11	581,364	52,851			21.32
Total	**15**	**2,727,270**				**100**
S = 229.894		R-sq: 78.68%		R-sq(adj): 70.93%		
				$\sigma_{Flexural} = \mathbf{22 + 30.56}I - \mathbf{59.7}U - \mathbf{46.7}d - \mathbf{0.81}v$		(5)

Interestingly, when the welding current increases in the examination rank, the tensile strength, yield strength, elongation, and flexural strength also increase, as shown in Equations (2)–(5). This is because a higher heat input during welding significantly affects the penetration capability of the weld. High heat input can enhance the penetration of the weld, ensuring a strong bond with the base material. The formula for calculating heat input is described as follows [44]:

$$Q = k\frac{U \times I}{v}\ (\text{J.mm}^{-1}) \quad (6)$$

where k = 0.8 for MIG welding, v is the travel speed (mm/s).

A good heat input could lead to reasonable penetration depth; however, if the heat input is excessively high, it can lead to dilution and damage to the base material. Moreover, if the heat distribution is good, it could lead to better melting or leaking of the base materials.

The electrical stick-out value strongly impacts the heat input distribution. Further, with the d factor's negative value, the arc length increases when the electrode stick-out increases. This leads to energy dispersing over a larger area and decreases the heat density at the contact point, reducing the arc temperature. In addition, as the electrode stick-out increases, the resistance of the electrode also increases. This reduces the efficiency of converting the electric current into thermal energy at the welding point, diminishing the ability to melt the base and filler metals. An increased arc length also reduces the arc pressure. Lower pressure results in less penetration of the molten metal into the base metal, thus reducing the weld penetration and mechanical properties [45].

Figures 5–8 show the main effect plot with the "larger is better" option for the mechanical values of the dissimilar weld joint between SUS 201 and C20. These figures indicate that the optimal parameters for the highest tensile test values are a welding current of 110 A, a welding voltage of 15 V, a stick-out of 10 mm, and a welding speed of 500 mm.min^{-1}. This parameter set's predicted UTS, yield strength, and elongation correspond to 442.19 MPa, 317.46 MPa, and 41.7%. The optimal parameters of 1742.53 MPa for flexural strength could be achieved with a welding current of 110 A, a welding voltage of 15 V, a stick-out of 12 mm, and a welding speed of 500 mm.min^{-1}. These parameter sets are compared to the validation experiment in the following section.

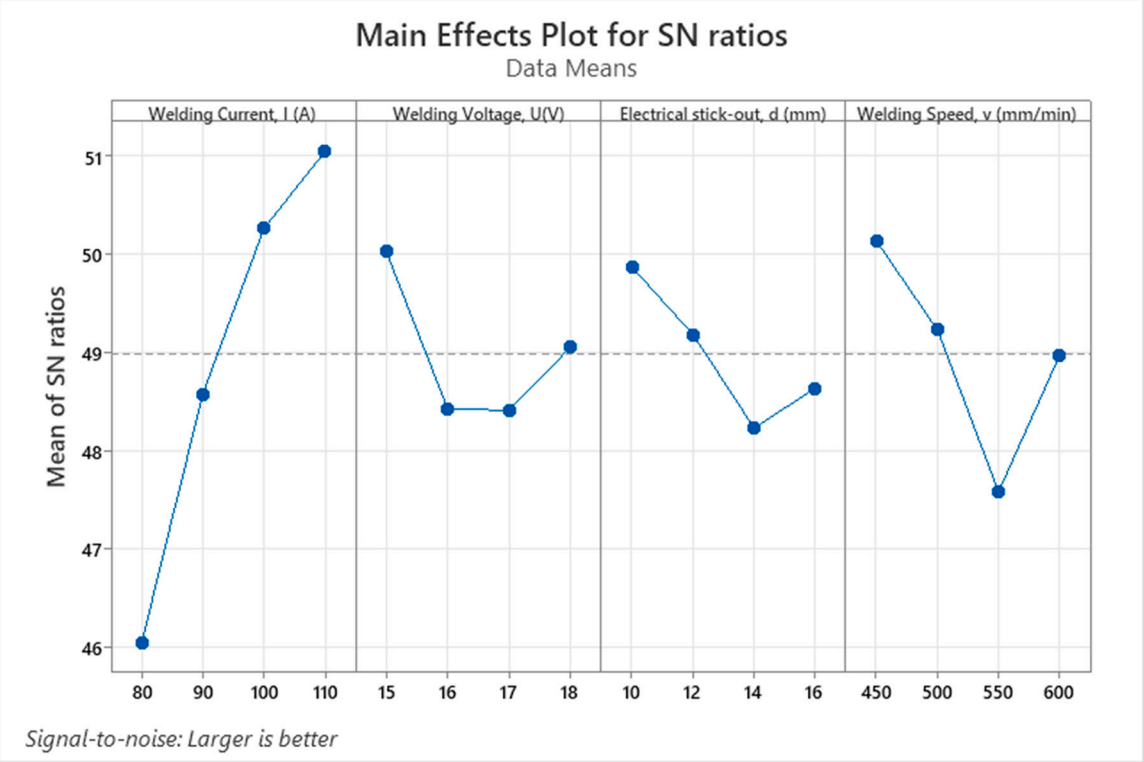

Figure 5. Main effects plot for S/N ratios for tensile strength.

The fracture location of a weld sample after tensile and bending tests is shown in Figure 9. In the tensile test, the samples fail in the area beside the weld bead due to the sensitivity of the heat-affected zone. There are no cracks when the samples are bent under the bending test, indicating the excellent penetration of the welding joints.

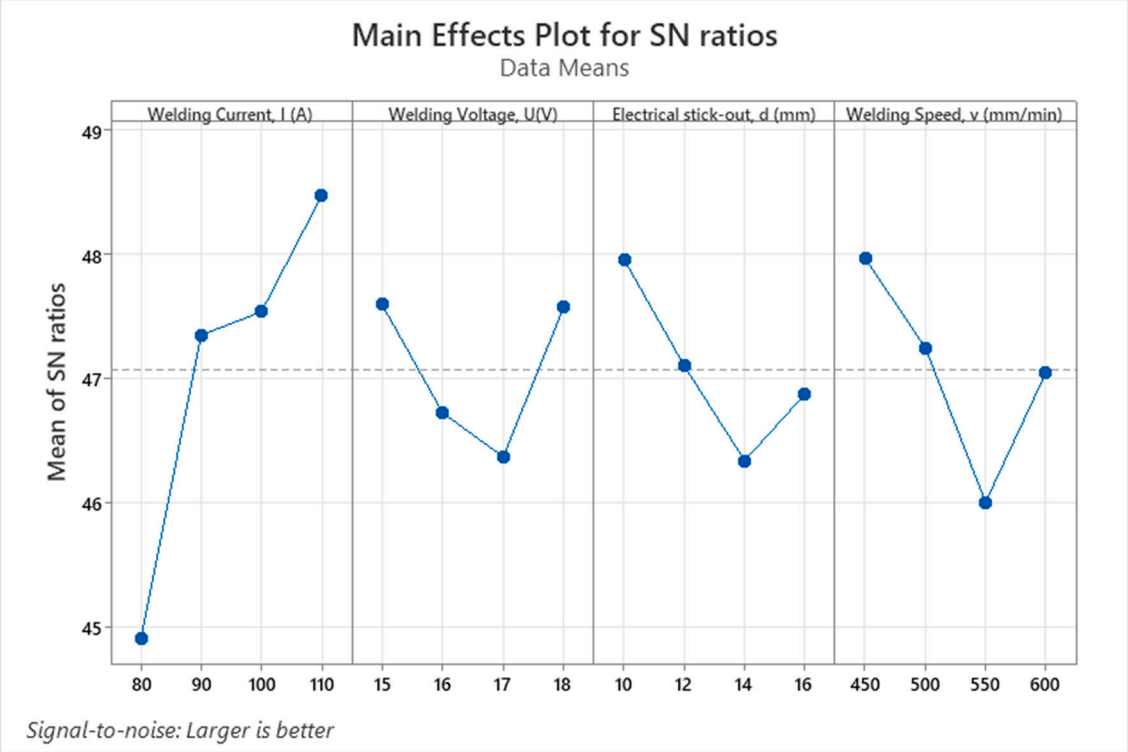

Figure 6. Main effects plot for S/N ratios for yield strength.

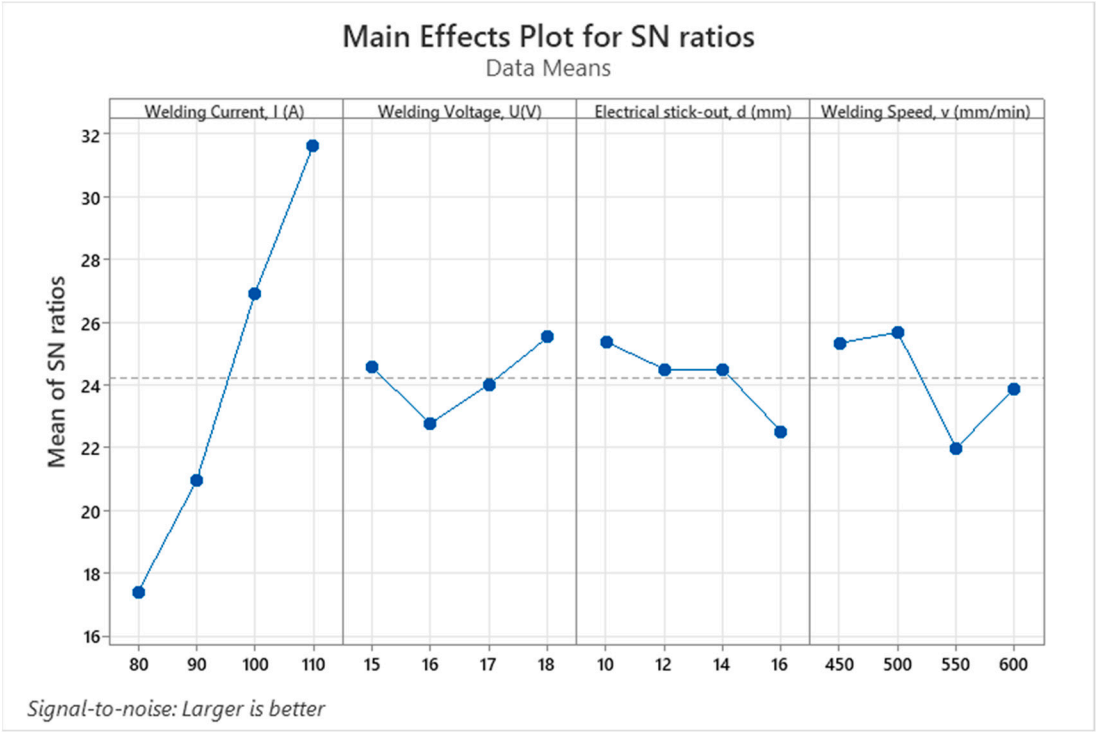

Figure 7. Main effects plot for S/N ratios for elongation.

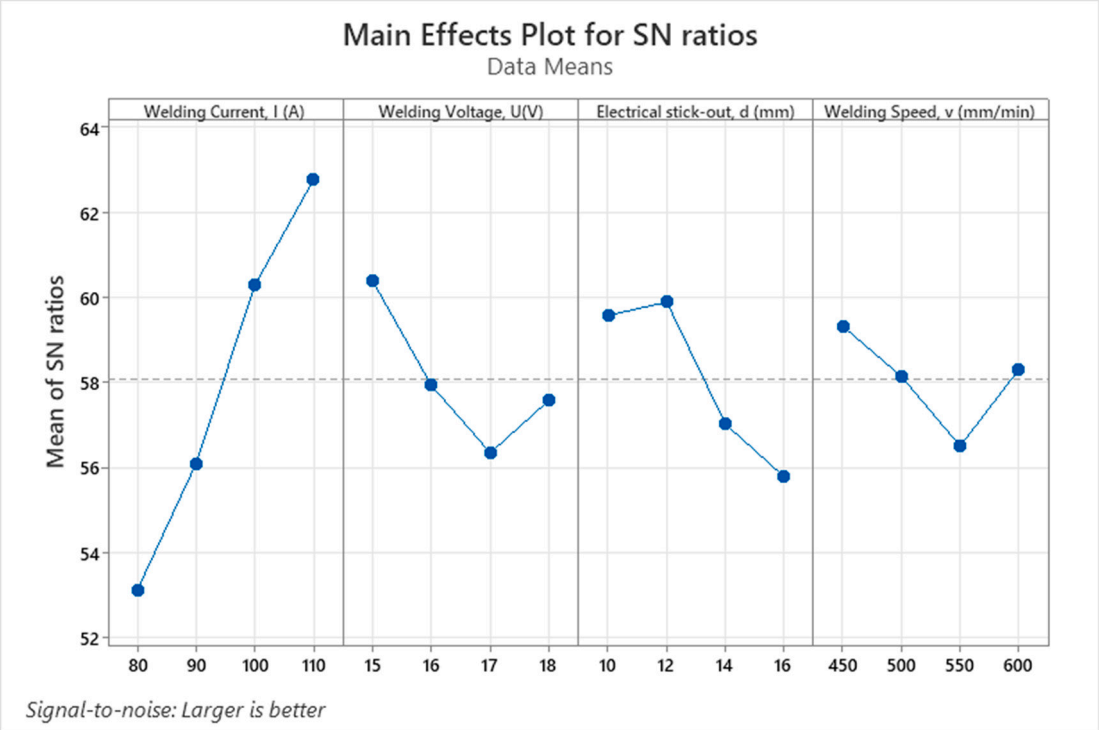

Figure 8. Main effects plot for S/N ratios for flexural strength.

Figure 9. Sample after test: (**a**) tensile test, and (**b**) bending test.

3.3. Validation Experiments

To substantiate the above conclusions based on the optimal parameters analyzed using the Taguchi method and ANOVA, exploratory experiments were conducted to provide an objective perspective on the optimal results and to enhance the reliability of these optimal parameters. The samples were newly welded using the previous optimal parameters.

The results of the comparison table of optimal parameters and experimental parameters are shown in Table 8. The experimental validation step is crucial, and it is recommended that it be conducted to conclude the entire experiment. The validation UTS value is 452.78 ± 3.35 MPa, which is even higher than the predicted value of 442.19. This result indicates the effectiveness of the Taguchi method in the optimization process. It is worth noting that the validation value is also higher than the highest value of the previous experiment samples,

which is only 388.29 MPa. In other words, applying the Taguchi method leads to a 16.7% improvement in the UTS value. The elongation at break value experiences a slight reduction, comparable to the predicted value. The validation of yield strength and flexural strength also indicated an improvement of 26% and 9.86%, respectively, to the highest value from previous experiments. This means that Taguchi's optimal parameters successfully increase the mechanical properties of dissimilar SUS 201 stainless steel and C20 steel. Notably, SUS 304 and SUS 201 are austenitic steel, while AISI 1018. SAE 1020 and C20 steel are similar low-carbon steel with about 0.2% carbon. Interestingly, this result is slightly higher than the Khdir et al. [27] report which reports the highest UTS value of 416 MPa of dissimilar welding between carbon steel AISI 1018 and stainless steel AISI 304. Dos Santos et al. [46] investigated the dissimilar welding between carbon steel SAE 1020 and stainless steel AISI 304 via the ultra-high-frequency-pulsed GTAW welding method. They reported a good-to-excellent UTS value of 450 MPa, which is comparable to this study's results.

Table 8. Comparison table of results for optimal parameters and experimental parameters.

Properties	Predicted Optimal Parameters	Validation Experiments	Average of Validation Experiments	Highest Values from Previous Experiments
Tensile Strength (MPa)	442.19	449.0 453.96 455.37	452.78 ± 3.35	388.29
Yield Strength (MPa)	317.459	369.6 386.8 367.54	374.65 ± 10.58	279.2
Elongation (%)	41.7	41.0 36.5 38.14	38.55 ± 2.28	42.25
Flexural Strength (MPa)	1742.53	1772.15 1742.86 1755.32	1756.78 ± 14.70	1599.02

3.4. Macrostructure and Microstructure Analysis

In this section, the microstructural examination helps reinforce the above arguments. The weld's mechanical qualities, including strength, ductility, hardness, and crack resistance, can be influenced by its microstructure. As a result, microstructure analysis is critical for determining the quality of the weld and ensuring performance.

Figure 10 shows the structures of dissimilar welding joints between C20 steel and SUS 201 steel. Figure 10a shows that the weld joint macrostructure includes the base metal (BM), HAZ, fusion boundary (FB), and weld metal (WM). With a C20 steel base, Figure 10b reveals the typical two-phase low-carbon steel microstructure comprising ferrite and pearlite. Ferrite is a soft and ductile phase, while pearlite is harder and more brittle. The proportion of ferrite to pearlite influences the material's strength and ductility. With SUS 201 steel base, Figure 10c displays the austenitic structure characteristic of SUS 201 steel, featuring twin crystal boundaries. Austenite is the ductile phase of steel at room temperature.

Due to the heat from the welding process, the microstructure of C20 steel in the HAZ changes, with the ferrite grain becoming more considerable, as illustrated in Figure 10d. Figure 10e shows the formation of δ-ferrite within the SUS 201 structure during welding. The presence of δ-ferrite phases is due to phase transformation from the austenite phase, showing the specific phase of austenite stainless steel dissimilar welding joints [47]. This phenomenon reduces the ability to maintain an entirely austenitic structure, allowing δ-ferrite to form when Cr predominates during cooling. The formation of δ-ferrite in the weld metal helps prevent hot cracking by providing alternate diffusion paths for elements and reducing thermal stress during cooling [48]. Notably, the heat-affected zones in Figure 10d,e are the sensitivity zones with many brittle phases, leading to the fracture of the test samples, as shown in Figure 9.

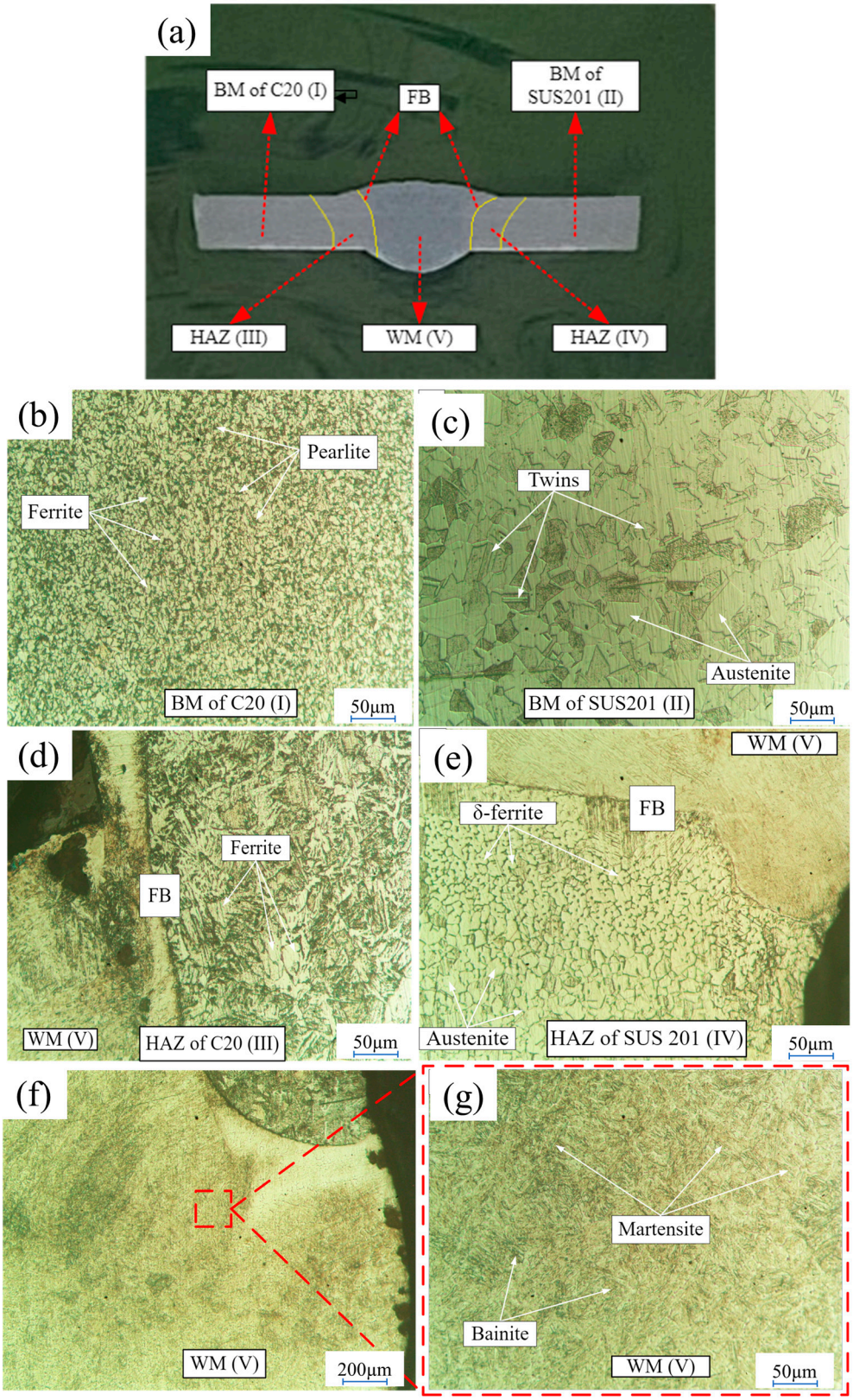

Figure 10. Structures of dissimilar welding joint between C20 steel and SUS 201 steel: (**a**) Marcrostructure, (**b**) Base metal of C20, (**c**) Base metal of SUS 201, (**d**) Weld joint interface and heat-affected zone of welded C20, (**e**) Weld joint interface and heat-affected zone of SUS 201, (**f**) Weld metal 5×, and (**g**) Weld metal 20×.bain.

Figure 10f,g show that a martensitic structure is observed in the WM. Bainite structure is also found in this area. The microstructure of the WM consists of martensite and bainite microstructures. The formation of these microstructures is determined by the welding temperature and the cooling rate during the welding process, which was also revealed by Guo et al. [49]. Moreover, martensite is a challenging and brittle phase of steel that forms due to rapid cooling during welding. The WM zone has a martensite and bainite microstructure due to fast heating and cooling during the welding process, which is consistent with the study by Khan et al. [25]. The presence of martensite can enhance the weld's tensile strength and hardness but also increases the risk of cracking. Additionally, a bainitic structure has also formed in the weld metal zone. Bainite has high tensile strength and hardness, enhancing the material's load-bearing capacity. Furthermore, this structure has better toughness than martensite, reducing the risk of brittle fracture.

4. Conclusions

This study examined the effects of stick-out, speed, voltage, and welding intensity on the mechanical characteristics and structure of MIG welding on SUS 201 stainless steel and C20 steel. The experiment findings are optimized by applying the Taguchi method in this study. Notable observations can be drawn to a close:

A higher current increases the heat generated during welding, making melting the filler and base metal easier. In the tensile test, the effect of welding current is most substantial compared to the welding voltage, stick-out, and welding speed. The welding voltage has the lowest impact level.

Besides the base metals' ferrite, pearlite, and austenite phases, there are martensite and bainite microstructures on the weld bead area. Moreover, fine columnar dendrites appear at the fusion areas, and δ-ferrite phases with dark lines and shapes gather between the fusion line and the austenite phases.

Optimal parameters for UTS, yield strength, and elongation values are a welding current of 110 amp, a voltage of 15 V, a welding speed of 500 mm.min^{-1}, and a stick-out of 10 mm. The confirmation of the UTS, yield strength, and elongation values are 452.78 MPa, 374.65 MPa, and 38.55%, respectively, which are consistent with the predicted value calculated from the Taguchi method, indicating the benefit of the Taguchi method.

The optimal parameters for flexural strength are a welding current of 110 amp, an arc voltage of 15 V, a welding speed of 500 mm.min^{-1}, and a stick-out of 12 mm. The confirmation of the flexural strength is 1756.78 MPa, which is higher than the other samples. In the flexural test, the welding current is the most critical factor impacting flexural strength. Moreover, flexural strength is less sensitive to the welding speed than other parameters. Further investigation could consider the effects of the thermal annealing process on the mechanical properties of the dissimilar weld joints. The study's findings could provide helpful insight into the dissimilar welding field.

Author Contributions: T.T.N., V.H.H. and V.-T.N.: conceptualization, funding acquisition; T.T.N. and V.-T.N.: writing original draft, investigation; T.T.N., V.H.H. and V.T.T.N.: analyzing, visualization, and project administration; V.T.T.N., T.T.N. and V.H.H.: writing, review, and editing. All authors have read and agreed to the published version of the manuscript.

Funding: This research received no external funding.

Institutional Review Board Statement: Not applicable.

Informed Consent Statement: Not applicable.

Data Availability Statement: The raw data supporting the conclusions of this article will be made available by the authors upon request.

Acknowledgments: We would like to express our deep gratitude to the Material Testing Laboratory at Ho Chi Minh City University of Technology and Education for sponsoring the equipment for the experiment. We also thank Thanh-Lich Nguyen, Tran-Trung-Kien Nguyen, and Van Hien-Nguyen for supporting us during the research process.

Conflicts of Interest: The authors declare no conflicts of interest.

References

1. *UNI 7874:1979*; Forged Unalloyed or Special-Alloyed, Quenched and Tempered or Normalized Steel Flat Products. Ente Nazionale Italiano di Unificazione: Milan, Italy, 1979.
2. *JIS G 4303*; Stainless Steel Bars. JSA: Tokyo, Japan, 2023.
3. *AWS A5.18/A5.18M*; Specification for Carbon Steel Electrodes and Rods for Gas Shielded Arc Welding. American Welding Society: Danvers, MA, USA, 2021.
4. Wang, P.; Chen, X.; Pan, Q.; Madigan, B.; Long, J. Laser welding dissimilar materials of aluminum to steel: An overview. *Int. J. Adv. Manuf. Technol.* **2016**, *87*, 3081–3090. [CrossRef]
5. Shah, L.H.; Ishak, M. Review of Research Progress on Aluminum–Steel Dissimilar Welding. *Mater. Manuf. Process.* **2014**, *29*, 928–933. [CrossRef]
6. Morishige, T.; Kawaguchi, A.; Tsujikawa, M.; Hino, M.; Hirata, T.; Higashi, K. Dissimilar Welding of Al and Mg Alloys by FSW. *Mater. Trans.* **2008**, *49*, 1129–1131. [CrossRef]
7. Joseph, A.; Rai, S.K.; Jayakumar, T.; Murugan, N. Evaluation of residual stresses in dissimilar weld joints. *Int. J. Press. Vessel. Pip.* **2005**, *82*, 700–705. [CrossRef]
8. Kumar, N.; Pandey, C.; Kumar, P. Dissimilar Welding of Inconel Alloys With Austenitic Stainless-Steel: A Review. *J. Press. Vessel. Technol.* **2023**, *145*, 011506. [CrossRef]
9. Radhakrishnan, V.M. *Welding Technology and Design*; New Age International: Delhi, India, 2005.
10. Srivastava, D.; Chadha, U.; Gunreddy, N.; Saini, N.K.; Matara, N.N.; Machindar, O.; Mishra, U.V.; Khanna, M.; Kishore, S.R.; Selvaraj, S.K. A brief review on the Tube-to-Tube plate welding process. *Mater. Today Proc.* **2022**, *64*, 870–882. [CrossRef]
11. Srinivasan, P.B.; Muthupandi, V.; Dietzel, W.; Sivan, V. An assessment of impact strength and corrosion behaviour of shielded metal arc welded dissimilar weldments between UNS 31803 and IS 2062 steels. *Mater. Des.* **2006**, *27*, 182–191. [CrossRef]
12. Ul-Hamid, A.; Tawancy, H.M.; Abbas, N.M. Failure of weld joints between carbon steel pipe and 304 stainless steel elbows. *Eng. Fail. Anal.* **2005**, *12*, 181–191. [CrossRef]
13. Farman, N.F.; Alasadi, S.; Redha, Z.A.A. A Review of Advances in Pressurizer Response Research for Pressurized Water Reactor Systems. *Int. J. Simul. Syst. Sci. Technol.* **2018**, *19*, 1–11. [CrossRef]
14. Abson, D.J.; Rothwell, J.S. Review of type IV cracking of weldments in 9–12%Cr creep strength enhanced ferritic steels. *Int. Mater. Rev.* **2013**, *58*, 437–473. [CrossRef]
15. Yan, S.; Li, Z.; Song, L.; Zhang, Y.; Wei, S. Research and development status of laser micro-welding of aluminum-copper dissimilar metals: A review. *Opt. Lasers Eng.* **2023**, *161*, 107312. [CrossRef]
16. Narasimhan, P.N.; Mehrotra, S.; Raja, A.R.; Vashista, M.; Yusufzai, M.Z.K. Development of hybrid welding processes incorporating GMAW and SMAW. *Mater. Today Proc.* **2019**, *18*, 2924–2932. [CrossRef]
17. White, S.A.; Prachyabrued, M.; Chambers, T.L.; Borst, C.W.; Reiners, D. Low-cost simulated MIG welding for advancement in technical training. *Virtual Real.* **2011**, *15*, 69–81. [CrossRef]
18. Jagadeesha, T.; Nikam, M.; Mothilal, T.; Raj Kamal, M.D. Advancements in Welding Techniques: Surface and Mechanical Property Insights. In *New Materials, Processing and Manufacturability: Fabrication and Processing of Advanced Materials*; Scrivener Publishing LLC: Beverly, MA, USA, 2024; pp. 269–286. [CrossRef]
19. Afriansyah, A.A. Dissimilar metal welding using Shielded metal arc welding: A Review. *Technol. Rep. Kansai Univ.* **2020**, *62*, 1935–1948.
20. Kil Kim, J.; Hong, S.G.; Kang, K.B.; Kang, C.Y. Microstructure and high temperature properties of the dissimilar weld between ferritic stainless steel and carbon steel. *Met. Mater. Int.* **2009**, *15*, 843–849. [CrossRef]
21. Ranjbarnodeh, E.; Serajzadeh, S.; Kokabi, A.H.; Fischer, A. Effect of welding parameters on residual stresses in dissimilar stainless steel joint to carbon steel. *J. Mater. Sci.* **2011**, *46*, 3225–3232. [CrossRef]
22. Abioye, T.E.; Ariwoola, O.E.; Ogedengbe, T.I.; Farayibi, P.K.; Gbadeyan, O.O. Effects of Welding Speed on the Microstructure and Corrosion Behavior of Dissimilar Gas Metal Arc Weld Joints of AISI 304 Stainless Steel and Low Carbon Steel. *Mater. Today Proc.* **2019**, *17*, 871–877. [CrossRef]
23. Huang, C.-H.; Huang, C.-H.; Hou, C.-H.; Hou, C.-H.; Hsieh, T.-S.; Hsieh, T.-S.; Tsai, L.; Tsai, L.; Chiang, C.-C.; Chiang, C.-C. Investigation of distinct welding parameters on mechanical and corrosion properties of dissimilar welded joints between stainless steel and low carbon steel. *Sci. Prog.* **2022**, *105*, 00368504221126795. [CrossRef]
24. Ogedengbe, T.I.; Abioye, T.E.; Ekpemogu, A.I. Investigation of mechanical properties and parametric optimization of the dissimilar GTAW of AISI 304 stainless steel and low carbon steel. *World J. Eng.* **2018**, *15*, 584–591. [CrossRef]
25. Khan, M.; Dewan, M.W.; Sarkar, M.Z. Effects of welding technique, filler metal and post-weld heat treatment on stainless steel and mild steel dissimilar welding joint. *J. Manuf. Process.* **2021**, *64*, 1307–1321. [CrossRef]
26. Abioye, T.E.; Kanu, C.O.; Ogedengbe, T.I.; Adebiyi, D.I. Parametric optimisation of gas metal arc dissimilar welding on AISI 304 stainless steel and low carbon steel. *Int. J. Microstruct. Mater. Prop.* **2019**, *14*, 155. [CrossRef]
27. Khdir, Y.K.; Kako, S.A.; Gardi, R.H. Study of Welding Dissimilar Metals—Low-carbon Steel AISI 1018 and Austenitic Stainless Steel AISI 304. *Polytech. J.* **2020**, *10*, 1. [CrossRef]

28. Prabakaran, M.P.; Kannan, G.R. Effects of post-weld heat treatment on dissimilar laser welded joints of austenitic stainless steel to low carbon steel. *Int. J. Press. Vessel. Pip.* **2021**, *191*, 104322. [CrossRef]
29. Prabakaran, M.; Kannan, G.R.; Pandiyarajan, R. Effects of Welding Speed on Microstructure and Mechanical Properties of CO_2 Laser Welded Dissimilar Butt Joints between Low Carbon Steel and Austenitic Stainless Steel. *Adv. Mater. Process. Technol.* **2020**, *8*, 1–12. [CrossRef]
30. Bin Matlan, M.J.; Mohebbi, H.; Pedapati, S.R.; Awang, M.B.; Ismail, M.C.; Kakooei, S.; Dan, N.E.; Bin Matlan, M.J.; Mohebbi, H.; Pedapati, S.R.; et al. Dissimilar Friction Stir Welding of Carbon Steel and Stainless Steel: Some Observation on Microstructural Evolution and Stress Corrosion Cracking Performance. *Trans. Indian Inst. Met.* **2018**, *71*, 2553–2564. [CrossRef]
31. Muzakki, H.; Zubairi, I.; Mubarok, K. The effect of argon gas pressure and MIG (metal inert gas) welding parameters on dissimilar steel. In *AIP Conference Proceedings*; AIP Publishing: Melville, NY, USA, 2024; Volume 2927. [CrossRef]
32. Sakthivel, R.; Venkadeshwaran, P.; Sridev, R.; Meeran, R.A.; Chandrasekaran, K. Effect of Welding Current, Arc Voltage and Gas Flow Rate on Depth of Penetration during MIG Welding of AA2014 Plate. *Int. J. Adv. Res. Technol.* **2015**, *2*, 30.
33. Shunmugasundaram, M.; Kumar, A.P.; Sankar, L.P.; Sivasankar, S. Optimization of process parameters of friction stir welded dissimilar AA6063 and AA5052 aluminum alloys by Taguchi technique. *Mater. Today Proc.* **2020**, *27*, 871–876. [CrossRef]
34. Roy, R.; St, C. *Design of Experiments Using The Taguchi Approach 16 Steps to Product and Process Improvement*; John Wiley & Sons: Hoboken, NJ, USA, 2001.
35. Mori, T.; Tsai, S.C. *Taguchi Methods*; ASME: New York, NY, USA, 2011; pp. 10016–15990.
36. Benlamnouar, M.F.; Hadji, M.; Badji, R.; Bensaid, N.; Saadi, T.; Laksir, Y.L.D.; Senouci, S. Optimization of TIG Welding Process Parameters for X70-304L Dissimilar Joint Using Taguchi Method. *Solid State Phenom.* **2019**, *297*, 51–61. [CrossRef]
37. Ramarao, M.; King, M.F.L.; Sivakumar, A.; Manikandan, V.; Vijayakumar, M.; Subbiah, R. Optimizing GMAW parameters to achieve high impact strength of the dissimilar weld joints using Taguchi approach. *Mater. Today Proc.* **2022**, *50*, 861–866. [CrossRef]
38. Behera, A. Optimization of process parameters in laser welding of dis-similar materials. *Mater. Today Proc.* **2020**, *33*, 5765–5769. [CrossRef]
39. Wichan, C.; Loeshpahn, S. Effect of Filler Alloy on Microstructure, Mechanical and Corrosion Behaviour of Dissimilar Weldment between Aisi 201 Stainless Steel and Low Carbon Steel Sheets Produced by a Gas Tungsten Arc Welding. *Adv. Mater. Res.* **2012**, *581–582*, 808–816. [CrossRef]
40. *ASTM E8/E8M-13*; Standard Test Methods for Tension Testing of Metallic Materials. ASTM: West Conshohocken, PA, USA, 2013.
41. *ASTM E290*; Standard Test Methods for Bend Testing of Material for Ductility. ASTM: West Conshohocken, PA, USA, 2022.
42. Zhang, Q.; Luo, Z.; Jang, B.-A.; Wang, Q.; Zhong, Z.; Jiang, H. A Study of Instantaneous Shear Mechanical Properties on the Discontinuity of Rock Mass Based on 3D Morphological Properties. *Geofluids* **2021**, *2021*, 5549223. [CrossRef]
43. Tran, V.T.; Le, M.H.; Vo, M.T.; Le, Q.T.; Hoang, V.H.; Tran, N.-T.; Nguyen, T.-A.; Nguyen, H.N.; Nguyen, V.T.T. Optimization design for die-sinking EDM process parameters employing effective intelligent method. *Cogent Eng.* **2023**, *10*, 2264060. [CrossRef]
44. Ogundimu, E.O.; Akinlabi, E.T.; Erinosho, M.F. An experimental study on the effect of heat input on the weld efficiency of TIG-MIG hybrid welding of type 304 austenitic stainless steel. In *Journal of Physics: Conference Series*; IOP Publishing: Bristol, UK, 2019; Volume 1378, p. 022075. [CrossRef]
45. e Silva, R.H.G.; Paes, L.E.d.S.; Barbosa, R.C.; Sartori, F.; Schwedersky, M.B. Assessing the effects of solid wire electrode extension (stick out) increase in MIG/MAG welding. *J. Braz. Soc. Mech. Sci. Eng.* **2018**, *40*, 31. [CrossRef]
46. dos Santos, F.J.; Dutra, G.B.; da Cunha, T.V. Microstructural and mechanical evaluation of a dissimilar joining between SAE 1020 and AISI 304 steel obtained via ultra-high-frequency-pulsed GTAW. *J. Braz. Soc. Mech. Sci. Eng.* **2019**, *41*, 26. [CrossRef]
47. Hsieh, C.-C.; Lin, D.-Y.; Chen, M.-C.; Wu, W. Precipitation and strengthening behavior of massive δ-ferrite in dissimilar stainless steels during massive phase transformation. *Mater. Sci. Eng. A* **2008**, *477*, 328–333. [CrossRef]
48. Kou, S. *Welding Metallurgy*, 2nd ed.; John Wiley & Sons, Inc.: Hoboken, NJ, USA, 2003.
49. Guo, Z.; Ma, T.; Yang, X.; Li, W.; Xu, Q.; Li, Y.; Li, J.; Vairis, A. Comprehensive investigation on linear friction welding a dissimilar material joint between Ti17(α+β) and Ti17(β): Microstructure evolution, failure mechanisms, with simultaneous optimization of tensile and fatigue properties. *Mater. Sci. Eng. A* **2024**, *909*, 146818. [CrossRef]